Advances in Nano Research, *Vol. 19, No. 2 (2025) 153-164*
https://doi.org/10.12989/anr.2025.19.2.153

Investigation of the smart NPR cellular sandwich plate in large amplitude vibration under the effect of different boundary conditions

Farzad Ebrahimi*[1], Mohammad Mahinzare[2] and Seyede Zahra Mirsadoghi[1]

[1]*Department of Mechanical Engineering, Faculty of Engineering, Imam Khomeini International University, Qazvin, Iran*
[2]*School of Mechanical Engineering, College of Engineering, University of Tehran, Tehran, Iran*

(*Received February 19, 2025, Revised August 9, 2025, Accepted August 20, 2025*)

Abstract. This research models the novel smart NPR cellular plate's large amplitude oscillation utilizing the Mindlin plate theory. The plate consists of an Auxetic metamaterial core and smart composite layers. By using the micromechanical concept, one may ascertain the characteristics of the NPR cellular core and smart composite layers. Then, using von Karman nonlinearity terms and Hamilton's principle, the equations controlling the smart NPR cellular sandwich plates' behavior may be developed. The GDQM is then used to answer these mathematical problems. It is also possible to determine the smart NPR cellular plate's frequency ratio by taking the outside voltage. Each Figure also shows the calculated impacts of the NPR cellular geometrical properties and the NPR cellular layer thickness. All of these variables had an effect on the frequency ratio.
Keywords: composite; large amplitude; nonlinear vibration; NPR; smart GPL

1. Introduction

Because of distinctive characteristics and extensive uses, NPR cellular metamaterial frameworks are being studied by Yazdani Sarvestani *et al*. (2018), Huang *et al*. (2013), Wang *et al*. (2015), and Mahinzare *et al*. (2023). Following lateral compression, typical materials exhibit an increase in the axial direction (Poisson ratio with a positive value). In contrast, particular materials exhibit a negative Poisson ratio, known as "auxetic," which are typically found in the natural world, especially in minerals and epidermis (Evans, 1991). Yang *et al*. (2004) identified NPR cellular material's the uses, processes, and characteristics of NPR cellular material, particularly regarding negative Poisson ratios. Moreover, Ranjbar *et al*. (2016) improved the frequency range of laminated frameworks composed of anti-tetrachiral and hexagonal segments. This study concludes that the NPR cellular hexagon at low frequency is superior for reducing radiation noise. Quan *et al*. (2020) examined a sandwich plate's associated nonlinear dynamical responses, composed of NPR cellular, piezoelectric, and gold layers. Additionally, Nguyen and Pham (2018) analyzed the dynamic behavior of a rectangular-shaped plate using an NPR cellular core, employing Runge-Kutta and Galerkin methods to solve the governing equations. Jiang and Hu (2017) also explored the evaluation of low-velocity effects on the sandwich plate with the NPR cellular core. Furthermore, Mazloumi *et al*. (2018) calculated the unconstrained vibration of a two-dimensional honeycomb-shaped plate and determined the NPR cellular radiative frequencies of the composite plate. Recently, smart materials have gained popularity, as they generate electro-elastic responses due to charge generation followed by elastic deformation. Several investigators followed by elastic deformation. Several investigators have examined the behaviors of smart materials for this particular reason (Mahinzare *et al*. 2019, Hosseini *et al*. 2018). For instance, Ebrahimi and Dabbagh (2019) evaluated the wave transmission properties of smart frameworks. Furthermore, Ebrahimi and Barati (2016) investigated the vibration of piezoelectric beams using nonlocal elasticity theory (NET) and higher-order shear deformation theory (HSDT), as well as a smart constitutive model for assessing the impact of magneto-electric fields on the beam's natural frequencies. Moreover, Ghorbanpour Arani *et al*. (2017) revealed the flexural wave dispersal properties of electromagnetic plates through their viscoelastic characteristics.

Several investigators (Hua and Lam 2001, Mohammadi *et al*. 2017, Ilkhani and Hosseini-Hashemi 2016) have identified vibratory responses as significant structural assessments. For example, Jafari *et al*. (2014) provided insights into the nonlinear oscillation of functionally graded (FG) plates with piezoelectric coatings, studying the effect of external voltage on their natural frequencies. In addition, Malekzadeh (2008) studied the vibrational behavior of a skew plate through the differential quadrature method (DQM), particularly under significant amplitudes and First-Order Shear Deformation Theory (FSDT). Furthermore, Sundararajan *et al*. (2005) studied the nonlinear vibrational behavior of FG skew and rectangular plates subjected to varying temperatures and environmental conditions. Ebrahimi and Zia (2015) employed Timoshenko beam theory to examine large amplitude oscillations in FG porous beams. Using an analytical approach, Rachid *et al*. (2014) presented nonlinear vibrations of FG disks, while Chen and Li (2017) analyzed the aeroelastic oscillation effects on cylindrical shells exposed to supersonic airflow.

Shariyat *et al*. (2010) developed wave dispersion and

*Corresponding author, Ph.D.,
E-mail: febrahimy@eng.ikiu.ac.ir

ISSN: 2287-237X (Print), 2287-2388 (Online)

nonlinear oscillation in thick FGM cylindrical shells, utilizing their temperature-dependent characteristics. Shen and Xiang (2014) explored large amplitude vibrations of cylindrical frames made from CNT-reinforced nano-composites under thermal environments based on elastic media. Ebrahimi and Rastgoo (2009) also calculated the nonlinear vibrations of smart FG circular plates with piezoelectric coatings. Mahinzare *et al*. (2024) analysed the nonlinear oscillation behavior of an orthotropic FG circular cylindrical shell using shear deformation theory. Chen and Kitipornchai (2017) discussed post-buckling and nonlinear oscillation in CNT-reinforced nanoporous FG beams derived from porosity analysis. Sh *et al*. (2022) provided insights into nonlinear responses during transient and unconstrained vibrations of a smart FG plate with pores while considering the effects of magneto-electric fields. Notably, none of the aforementioned studies have examined the nonlinear vibrations of a plate composed of a smart composite and an NPR cellular core.

This manuscript is the first to present a novel investigation utilizing Mindlin plate theory to calculate the large amplitude vibrations of a new smart composite plate. The material of this smart sandwich plate consists of two smart composite layers with an NPR cellular core. The governing equations and relevant boundary conditions for this innovative NPR cellular smart sandwich plate were determined utilizing von Karman geometrical nonlinearity and Hamilton's principle and calculated by the Generalized DQM. The frequency ratio of the NPR cellular smart sandwich plate could be determined as a function of the geometrical parameters of the NPR cellular structure and the external voltage incorporates to the smart layer. Unlike previous works, in this research we aim to model, the nonlinear vibrations of smart composite plates incorporating NPR (Negative Poisson's Ratio) cellular cores using the Mindlin plate theory. The integration of auxetic materials and smart composites in a geometrically nonlinear framework developed a novel approach to tunable vibration characteristics by utilizing the external electrical stimuli. Also, mechanical and civil structures, particularly in adaptive structures in which tuning stiffness and frequency response are critical. Their unique and novel auxetic behavior also makes them suitable for advanced applications like morphing wings, sensors, actuators, and flexible electronics.

2. Formulation

2.1 Material characteristics

$$C_{11} = \frac{C_{11}^{p} C_{11}^{m}}{\eta C_{11}^{m} + (1-\eta) C_{11}^{p}} \tag{1.1}$$

$$C_{12} = C_{11}\left[\frac{\eta C_{12}^{p}}{C_{11}^{p}} + \frac{(1-\eta) C_{12}^{m}}{C_{11}^{m}}\right] \tag{1.2}$$

$$C_{13} = C_{11}\left[\frac{\eta C_{13}^{p}}{C_{11}^{p}} + \frac{(1-\eta) C_{13}^{m}}{C_{11}^{m}}\right] \tag{1.3}$$

$$C_{22} = \eta C_{22}^{p} + (1-\eta) C_{22}^{m} + \frac{C_{12}^{2}}{C_{11}} - \frac{\eta\left(C_{12}^{p}\right)^{2}}{C_{11}^{p}} - \frac{(1-\eta)(C_{12}^{m})^{2}}{C_{11}^{m}} \tag{1.4}$$

$$C_{23} = \eta C_{23}^{p} + (1-\eta) C_{23}^{m} + \frac{C_{12} C_{13}}{C_{11}} - \frac{\eta C_{12}^{p} C_{13}^{p}}{C_{11}^{p}} - \frac{(1-\eta) C_{12}^{m} C_{13}^{m}}{C_{11}^{m}} \tag{1.5}$$

$$C_{33} = \eta C_{33}^{p} + (1-\eta) C_{33}^{m} + \frac{C_{13}^{2}}{C_{11}} - \frac{\eta\left(C_{13}^{p}\right)^{2}}{C_{11}^{p}} - \frac{(1-\eta)(C_{13}^{m})^{2}}{C_{11}^{m}} \tag{1.6}$$

$$C_{44} = \eta C_{44}^{p} + (1-\eta) C_{44}^{m} \tag{1.7}$$

$$C_{55} = \frac{A}{B^{2} + AC} \tag{1.8}$$

$$C_{66} = \frac{C_{66}^{p} C_{66}^{m}}{\eta C_{66}^{m} + (1-\eta) C_{66}^{p}} \tag{1.9}$$

$$e_{31} = C_{11}\left[\frac{\eta e_{31}^{p}}{C_{11}^{p}} + \frac{(1-\eta) e_{31}^{m}}{C_{11}^{m}}\right] \tag{1.10}$$

$$e_{32} = \eta e_{32}^{p} + (1-\eta) e_{32}^{m} + \frac{C_{12} e_{31}}{C_{11}} - \frac{\eta C_{12}^{p} e_{31}^{p}}{C_{11}^{p}} - \frac{(1-\eta) C_{12}^{m} e_{31}^{m}}{C_{11}^{m}} \tag{1.11}$$

$$e_{33} = \eta e_{33}^{p} + (1-\eta) e_{33}^{m} + \frac{C_{13} e_{31}}{C_{11}} - \frac{\eta C_{13}^{p} e_{31}^{p}}{C_{11}^{p}} - \frac{(1-\eta) C_{13}^{m} e_{31}^{m}}{C_{11}^{m}} \tag{1.12}$$

$$e_{24} = \eta e_{24}^{p} + (1-\eta) e_{24}^{m} \tag{1.13}$$

$$e_{15} = \frac{B}{B^{2} + AC} \tag{1.14}$$

$$s_{11} = \frac{C}{B^{2} + AC} \tag{1.15}$$

$$s_{22} = \eta s_{22}^{p} + (1-\eta) s_{22}^{m} \tag{1.16}$$

$$s_{33} = \eta s_{33}^{p} + (1-\eta) s_{33}^{m} + \frac{e_{31}^{2}}{C_{11}} - \frac{\eta\left(e_{31}^{p}\right)^{2}}{C_{11}^{p}} - \frac{(1-\eta)(e_{31}^{m})^{2}}{C_{11}^{m}} \tag{1.17}$$

$$A = \left[\frac{\eta C_{55}^{p}}{\left(e_{15}^{p}\right)^{2} + C_{55}^{p} s_{11}^{p}} + \frac{(1-\eta) C_{55}^{m}}{(e_{15}^{m})^{2} + C_{55}^{m} s_{11}^{m}}\right] \tag{1.18}$$

$$B = \left[\frac{\eta e_{15}^{p}}{\left(e_{15}^{p}\right)^{2} + C_{55}^{p} s_{11}^{p}} + \frac{(1-\eta) e_{15}^{m}}{(e_{15}^{m})^{2} + C_{55}^{m} s_{11}^{m}}\right] \tag{1.19}$$

$$C = \left[\frac{\eta s_{11}^{p}}{\left(e_{15}^{p}\right)^{2} + C_{55}^{p} s_{11}^{p}} + \frac{(1-\eta) s_{11}^{m}}{(e_{15}^{m})^{2} + C_{55}^{m} s_{11}^{m}}\right] \tag{1.20}$$

$$\rho = \eta \rho^{p} + (1-\eta)\rho^{m} \tag{1.21}$$

In which η is the percentage by volume of smart filler in the matrix.

2.2 NPR cellular core

In addition, the efficient characteristics of the NPR cellular core can be defined as (Mohammadpour and Taheri-Behrooz 2024):

Eqs. (2) reveal the actual mechanical characteristics of the NPR cellular core. In the equations mentioned earlier, geometrical variables such as angle (θ), e/l (vertical length to length), and t/l (thickness to length) are also input.

In the present study, the overall size-dependent behavior of the NPR was captured using a non-classical continuum model. However, the specific size effects directly induced by the geometric configuration of the NPR structure were not separately isolated, which can be explored in future works.

$$E_{11}^{a} = E\frac{\left(\frac{t}{l}\right)^{3} cos\,\theta}{\left(\frac{e}{l} + sin\,\theta\right) sin^{2}\,\theta} \tag{2.1}$$

$$E_{22}^{a} = E\frac{\left(\frac{t}{l}\right)^{3}\left(\frac{e}{l} + sin\,\theta\right)}{cos^{3}\,\theta} \tag{2.2}$$

$$G_{12}^{a} = E\frac{\left(\frac{t}{l}\right)^{3}\left(\frac{e}{l} + sin\,\theta\right)}{\left(\frac{e}{l}\right)^{2}\left(1 + \frac{2e}{l}\right) cos\,\theta} \tag{2.3}$$

$$\nu_{12}^{a} = \frac{cos^{2}\,\theta}{\left(\frac{e}{l} + sin\,\theta\right) sin\,\theta} \tag{2.4}$$

$$\rho_{a} = \rho\frac{\left(\frac{t}{l}\right)\left(\frac{e}{l} + 2\right)}{2\,cos\,\theta\left(\frac{e}{l} + sin\,\theta\right)} \tag{2.5}$$

Eqs. (2) reveal the actual mechanical characteristics of the NPR cellular core. In the equations mentioned earlier, geometrical variables such as angle (θ), e/l (vertical length to length), and t/l (thickness to length) are also input.

In the present study, the overall size-dependent behavior of the NPR was captured using a non-classical continuum model. However, the specific size effects directly induced by the geometric configuration of the NPR structure were not separately isolated, which can be explored in future works.

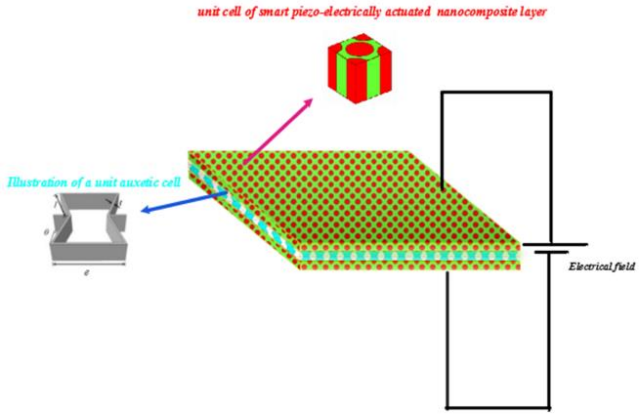

Fig. 1 The graphic of the smart sandwich plate with a NPR cellular core

2.3 Constitutive model

The subsequent equations can be derived from the electro-elastic constitutive modeling of a smart piezo-electrically operated sandwich plate (Sundararajan *et al.* 2005).

$$\sigma_{ij} = \left[C_{ijkl}\varepsilon_{kl} - e_{mij}E_{m}\right] \tag{3.1}$$

$$D_{i} = \left[e_{ikl}\varepsilon_{kl} + s_{im}E_{m}\right] \tag{3.2}$$

That the stresses, strain, and elasticity tensors are represented correspondingly by σ_{ij} ε_{kl} and C_{ijkl}. Additionally, D_i and E_m respectively indicate an electric displacement and field of electricity. Furthermore, s_{im} and e_{ikl} signify the dielectric coefficients and piezoelectric coefficients, respectively. Moreover, the connection between stress and strain of a smart sandwich plate that is piezoelectrically actuated is defined by the following formula:

$$\begin{Bmatrix}\sigma_{xx}\\ \sigma_{yy}\\ \sigma_{yz}\\ \sigma_{zx}\\ \sigma_{xy}\end{Bmatrix} = \left\{\begin{pmatrix} c_{11} & c_{12} & 0 & 0 & 0\\ c_{12} & c_{11} & 0 & 0 & 0\\ 0 & 0 & c_{55} & 0 & 0\\ 0 & 0 & 0 & c_{55} & 0\\ 0 & 0 & 0 & 0 & c_{66}\end{pmatrix}\begin{Bmatrix}\varepsilon_{xx}\\ \varepsilon_{yy}\\ \varepsilon_{yz}\\ \varepsilon_{zx}\\ \varepsilon_{xy}\end{Bmatrix} - \begin{pmatrix} 0 & 0 & e_{31}\\ 0 & 0 & e_{31}\\ 0 & e_{15} & 0\\ e_{15} & 0 & 0\\ 0 & 0 & 0\end{pmatrix}\begin{Bmatrix}E_x\\ E_y\\ E_z\end{Bmatrix}\right\}$$

$$\begin{Bmatrix}D_x\\ D_y\\ D_z\end{Bmatrix} = \left\{\begin{pmatrix} 0 & 0 & 0 & 0 & e_{15} & 0\\ 0 & 0 & 0 & e_{15} & 0 & 0\\ e_{31} & e_{31} & 0 & 0 & 0 & 0\end{pmatrix}\begin{Bmatrix}\varepsilon_{xx}\\ \varepsilon_{yy}\\ \varepsilon_{zz}\\ \varepsilon_{yz}\\ \varepsilon_{zx}\\ \varepsilon_{xy}\end{Bmatrix} - \begin{pmatrix} s_{11} & 0 & 0\\ 0 & s_{11} & 0\\ 0 & 0 & s_{33}\end{pmatrix}\begin{Bmatrix}E_x\\ E_y\\ E_z\end{Bmatrix}\right\} \tag{4}$$

2.4 Kinematic relations

Depending on the Mindlin plate theory, the displacement field of the smart composite plate could be written as (Reddy 2006):

$$U(x,y,z,t) = u_0(x,y,t) - z\,\psi_x(x,y,t) \tag{5.1}$$

$$V(x,y,z,t) = v_0(x,y,t) - z\,\psi_y(x,y,t) \tag{5.2}$$

$$W(x,y,z,t) = w(x,y,t) \tag{5.3}$$

where u_0 and v_0 depicted as the longitudinal and transverse movements, the lateral movement of the rectangular in-shape plate is additionally depicted by w. Moreover, the rotations of the transverse normal around the y and x axis are represented by ψ_x and ψ_y, in that order. Furthermore, an electrical potential $\Phi(x,z,t)$ is utilized for the smart sandwich plate. To achieve Maxwell's rule, the linear and harmonic components may be estimated as:

$$\Phi(x,y,z,t) = -cos(\zeta z)\phi(x,z,t) + \frac{2z}{h}V_0 \tag{6}$$

where $\zeta = \frac{\pi}{h}$ and the outside voltage is expressed by V_0. Furthermore, the strain terms may be articulated as:

$$\begin{Bmatrix}\varepsilon_{xx}\\ \varepsilon_{yy}\\ \varepsilon_{xy}\end{Bmatrix} = \begin{Bmatrix}\varepsilon^0_{xx}\\ \varepsilon^0_{yy}\\ \varepsilon^0_{xy}\end{Bmatrix} + z\begin{Bmatrix}k^b_{xx}\\ k^b_{yy}\\ k^b_{xy}\end{Bmatrix}, \begin{Bmatrix}\gamma_{xz}\\ \gamma_{yz}\end{Bmatrix} = \begin{Bmatrix}\gamma^0_{xz}\\ \gamma^0_{yz}\end{Bmatrix} \tag{7}$$

The strain components expressed in Eq. (7) are obtained by substituting the displacement field definitions from Eq. (5) into the nonlinear strain-displacement relations given in Eq. (8), considering von Karman geometric nonlinearity:

$$\begin{Bmatrix}\varepsilon^0_{xx}\\ \varepsilon^0_{yy}\\ \varepsilon^0_{xy}\end{Bmatrix} = \begin{Bmatrix}\frac{\partial u_0}{\partial x} + \frac{1}{2}\left(\frac{\partial w}{\partial x}\right)^2\\ \frac{\partial v_0}{\partial x} + \frac{1}{2}\left(\frac{\partial w}{\partial y}\right)^2\\ \frac{\partial u_0}{\partial y} + \frac{\partial v_0}{\partial x} + \frac{\partial w}{\partial x}\frac{\partial w}{\partial y}\end{Bmatrix},$$

$$\begin{Bmatrix}k^b_{xx}\\ k^b_{yy}\\ k^b_{xy}\end{Bmatrix} = \begin{Bmatrix}-\frac{\partial^2 w}{\partial x^2}\\ -\frac{\partial^2 w}{\partial y^2}\\ -\frac{\partial^2 w}{\partial x \partial y}\end{Bmatrix}, \begin{Bmatrix}k^s_{xx}\\ k^s_{yy}\\ k^s_{xy}\end{Bmatrix} = \begin{Bmatrix}\frac{\partial \psi_x}{\partial x}\\ \frac{\partial \psi_y}{\partial y}\\ \frac{\partial \psi_x}{\partial y} + \frac{\partial \psi_y}{\partial x}\end{Bmatrix}, \tag{8}$$

$$\begin{Bmatrix}\gamma^0_{xz}\\ \gamma^0_{yz}\end{Bmatrix} = \begin{Bmatrix}\frac{\partial w}{\partial x} + \psi_x\\ \frac{\partial w}{\partial y} + \psi_y\end{Bmatrix}$$

The electric field is generated by:

$$E_x = -\frac{\partial \Phi}{\partial x} = cos(\zeta z)\frac{\partial \phi}{\partial x} \tag{9.1}$$

$$E_y = -\frac{\partial \Phi}{\partial y} = cos(\zeta z)\frac{\partial \phi}{\partial y} \tag{9.2}$$

$$E_z = -\frac{\partial \Phi}{\partial z} = -\zeta\, sin(\zeta z)\phi - \frac{2V}{h} \tag{9.3}$$

Utilizing Hamilton's principle for the auxetic sandwich plate to achieve the following:

$$\int_0^t \delta(\Pi_S - \Pi_K + \Pi_W)dt = 0 \tag{10}$$

where Π_S, Π_K and Π_W, signify strain, kinetic effort, and external work, respectively. The calculation of strain energy is as follows:

$$\begin{aligned}\Pi_S &= \int_V (\sigma_{ij}\varepsilon_{ij})dV \\ &= \int_V \begin{pmatrix}\sigma_{xx}\varepsilon_{xx} + \sigma_{yy}\varepsilon_{yy} + \sigma_{xy}\varepsilon_{xy}\\ +\sigma_{xz}\varepsilon_{xz} + \sigma_{yz}\varepsilon_{yz}\\ -D_xE_x - D_yE_y - D_zE_z\end{pmatrix}dV\end{aligned} \tag{11}$$

The energy of strain is given by substituting Eqs. (5-7) into Eq. (9), which states:

$$\begin{aligned}\Pi_S = &\int_A \begin{pmatrix}N_{xx}\varepsilon^0_{xx} + M_{xx}\varepsilon^1_{xx}\\ +N_{yy}\varepsilon^0_{yy} + M_{yy}\varepsilon^1_{yy}\\ +2N_{xy}\varepsilon^0_{xy} + 2M_{xy}\varepsilon^1_{xy}\\ +Q_{xz}\gamma^0_{xz} + Q_{yz}\gamma^0_{yz}\end{pmatrix}dA \\ &+ \int_{-h/2}^{h/2}\int_A \begin{pmatrix}-D_x\, cos(\zeta z)\delta(\frac{\partial \phi}{\partial x})\\ -D_y\, cos(\zeta z)\delta(\frac{\partial \phi}{\partial y})\\ +D_z\, sin(\zeta z)\delta\phi\end{pmatrix}dAdz\end{aligned} \tag{12}$$

That the forces and moments would be expressed as:

$$\begin{aligned}(N_{xx}, N_{yy}, N_{xy}) &= \int_{-h/2}^{h/2}\{\sigma_{xx}, \sigma_{yy}, \sigma_{xy}\}dz \\ (M_{xx}, M_{yy}, M_{xy}) &= \int_{-h/2}^{h/2}\{\sigma_{xx}, \sigma_{yy}, \sigma_{xy}\}zdz \\ (Q_{xz}, Q_{yz}) &= \int_{-h/2}^{h/2}\{\sigma_{xz}, \sigma_{yz}\}dz\end{aligned} \tag{13}$$

Moreover, outside employment could be obtained as:

$$\delta\Pi_W = \frac{1}{2}\int_A \left(N^E_x\left(\frac{\partial w}{\partial x}\right)^2 + N^E_y\left(\frac{\partial w}{\partial y}\right)^2\right)dA \tag{14}$$

Wherein N^E_x and N^E_y represent the outside electrical charges in the *y* and *x* directions, in that order. Similarly, the kinetic energy would be determined as bellow:

$$\Pi_K = \frac{1}{2}\int_A \begin{pmatrix}I_0\left(\frac{\partial u_0}{\partial t}\right)^2 + I_0\left(\frac{\partial v_0}{\partial t}\right)^2 + I_0\left(\frac{\partial w}{\partial t}\right)^2\\ +I_2\left(\frac{\partial \psi_x}{\partial t}\right)^2 + I_2\left(\frac{\partial \psi_y}{\partial t}\right)^2\end{pmatrix}dA \tag{15}$$

The mass inertias are considered in the following form:

$$(I_0, I_1, I_2) = \int_{-h/2}^{h/2}(1, z, z^2)\rho(z)dz \tag{16}$$

By putting Eqs. (10-14) in Eq. (8), the motion equations of the smart auxetic plate can be represented as:

$$\frac{\partial N_{xx}}{\partial x} + \frac{\partial N_{xy}}{\partial y} = I_0\frac{\partial^2 u_0}{\partial t^2} \tag{17.1}$$

$$\frac{\partial N_{xy}}{\partial x}+\frac{\partial N_{yy}}{\partial y}=I_0\frac{\partial^2 v_0}{\partial t^2} \tag{17.2}$$

$$\begin{aligned}&\frac{\partial}{\partial x}\left(N_{xx}\frac{\partial w}{\partial x}+N_{xy}\frac{\partial w}{\partial y}\right)+\frac{\partial}{\partial y}\left(N_{xy}\frac{\partial w}{\partial x}+N_{yy}\frac{\partial w}{\partial y}\right)\\&+\frac{\partial Q_{xz}}{\partial x}+\frac{\partial Q_{yz}}{\partial y}-N^E\nabla^2 w=I_0\frac{\partial^2 w}{\partial t^2}\end{aligned} \tag{17.3}$$

$$\frac{\partial M_{xx}}{\partial x}+\frac{\partial M_{xy}}{\partial y}-Q_{xz}=I_0\frac{\partial^2 \psi_x}{\partial t^2} \tag{17.4}$$

$$\frac{\partial M_{xy}}{\partial x}+\frac{\partial M_{yy}}{\partial y}-Q_{yz}=I_0\frac{\partial^2 \psi_y}{\partial t^2} \tag{17.5}$$

$$\int_A\begin{pmatrix}cos(\zeta z)\dfrac{\partial D_x}{\partial x}+cos(\zeta z)\dfrac{\partial D_y}{\partial y}\\+\zeta\, sin(\zeta z)D_z\end{pmatrix}dA=0 \tag{17.6}$$

The force and moment are presented as follows:

$$\begin{Bmatrix}N_{xx}\\N_{yy}\\N_{xy}\end{Bmatrix}=\begin{pmatrix}\begin{pmatrix}A_{11}&A_{12}&0\\A_{21}&A_{22}&0\\0&0&A_{66}\end{pmatrix}\begin{Bmatrix}\dfrac{\partial u_0}{\partial x}+\dfrac{1}{2}\left(\dfrac{\partial w}{\partial x}\right)^2\\\dfrac{\partial v_0}{\partial x}+\dfrac{1}{2}\left(\dfrac{\partial w}{\partial y}\right)^2\\\dfrac{\partial u_0}{\partial y}+\dfrac{\partial v_0}{\partial x}+\dfrac{\partial w}{\partial x}\dfrac{\partial w}{\partial y}\end{Bmatrix}\\+\begin{pmatrix}A_{31}^e\\A_{31}^e\\0\end{pmatrix}\phi-\begin{pmatrix}N_x^E\\N_y^E\\0\end{pmatrix}\end{pmatrix} \tag{18}$$

$$\begin{Bmatrix}M_{xx}\\M_{yy}\\M_{xy}\end{Bmatrix}=\begin{pmatrix}\begin{pmatrix}D_{11}&D_{12}&0\\D_{21}&D_{22}&0\\0&0&D_{66}\end{pmatrix}\begin{Bmatrix}\dfrac{\partial \psi_x}{\partial x}\\\dfrac{\partial \psi_y}{\partial y}\\\dfrac{\partial \psi_x}{\partial y}+\dfrac{\partial \psi_y}{\partial x}\end{Bmatrix}\\+\begin{pmatrix}E_{31}^e\\E_{31}^e\\0\end{pmatrix}\phi-\begin{pmatrix}M_{bx}^E\\M_{by}^E\\0\end{pmatrix}\end{pmatrix} \tag{19}$$

$$\begin{Bmatrix}Q_{xz}\\Q_{yz}\end{Bmatrix}=\begin{pmatrix}\begin{pmatrix}A_{44}&0\\0&A_{55}\end{pmatrix}\begin{Bmatrix}\dfrac{\partial w}{\partial x}+\psi_x\\\dfrac{\partial w}{\partial y}+\psi_y\end{Bmatrix}-E_{15}^e\begin{Bmatrix}\dfrac{\partial \phi}{\partial x}\\\dfrac{\partial \phi}{\partial y}\end{Bmatrix}\end{pmatrix} \tag{20}$$

$$\int_A\left(\begin{Bmatrix}D_x\\D_y\end{Bmatrix}cos(\zeta z)\right)dA=\begin{pmatrix}E_{15}^e\begin{Bmatrix}\dfrac{\partial w}{\partial x}+\psi_x\\\dfrac{\partial w}{\partial y}+\psi_y\end{Bmatrix}-X_{11}^e\begin{Bmatrix}\dfrac{\partial \phi}{\partial x}\\\dfrac{\partial \phi}{\partial y}\end{Bmatrix}\end{pmatrix} \tag{21}$$

$$\int_A(D_z\,\zeta\, sin(\zeta z))\,dA=\left(E_{31}^e\left(\frac{\partial \psi_x}{\partial x}+\frac{\partial \psi_y}{\partial y}\right)-X_{33}^e\phi\right) \tag{22}$$

Where:

$$\begin{aligned}\begin{pmatrix}A_{11}&D_{11}\\A_{12}&D_{12}\\A_{44}&D_{44}\end{pmatrix}=\Bigg(&(1,z^2)\left\{2\int_{-\frac{h}{2}}^{-\frac{h}{2}+h_{SNC}}\begin{Bmatrix}c_{11}^{SNC}\\c_{12}^{SNC}\\c_{66}^{SNC}\end{Bmatrix}dz\right.\\&\left.+\int_{-\frac{h_{Auxetic}}{2}}^{\frac{h_{Auxetic}}{2}}\begin{Bmatrix}c_{11}^{Auxetic}\\c_{12}^{Auxetic}\\c_{66}^{Auxetic}\end{Bmatrix}dz\right\}\Bigg)\end{aligned} \tag{23}$$

$$\begin{aligned}E_{31}^e&=2\int_{-\frac{h}{2}}^{-\frac{h}{2}+h_{SNC}}e_{31}\zeta z\, sin(\zeta z)dz\\E_{15}^e&=2\int_{-h/2}^{-\frac{h}{2}+h_{SNC}}e_{15}\,cos(\zeta z)dz\\(X_{11}^e,X_{33}^e)&\\=2\int_{-h/2}^{-\frac{h}{2}+h_{SNC}}&(s_{11}\,cos^2(\zeta z),s_{33}\zeta^2\,sin^2(\zeta z))dz\end{aligned} \tag{24}$$

Also, outside forces and momentum can be designed using the exterior electrical work:

$$N^E=N_x^E=N_y^E=-2\int_{-h/2}^{-\frac{h}{2}+h_{SNC}}\left(e_{31}\frac{2V_0}{h_{SNC}}\right)dz \tag{25}$$

$$M^E=M_x^E=M_y^E=-2\int_{-h/2}^{-\frac{h}{2}+h_{SNC}}\left(e_{31}\frac{2V_0}{h_{SNC}}\right)zdz \tag{26}$$

Through replacing Eqs. (18) – (24) in Eqs. (17.1) - (17.6), The equations of the piezoelectrically actuated plate, expressed in terms of displacement, can be established as follows:

$$\begin{pmatrix}A_{11}\left(\dfrac{\partial^2 u_0}{\partial x^2}+\dfrac{\partial w}{\partial x}\dfrac{\partial^2 w}{\partial x^2}\right)\\+(A_{12}+A_{66})\left(\dfrac{\partial^2 v_0}{\partial x\partial y}+\dfrac{\partial w}{\partial y}\dfrac{\partial^2 w}{\partial x\partial y}\right)\\+A_{66}\left(\dfrac{\partial^2 u_0}{\partial y^2}+\dfrac{\partial w}{\partial x}\dfrac{\partial^2 w}{\partial y^2}\right)+A_{31}^e\dfrac{\partial \phi}{\partial x}\end{pmatrix}=I_0\frac{\partial^2 u_0}{\partial t^2} \tag{27.1}$$

$$\begin{pmatrix}A_{22}\left(\dfrac{\partial^2 v_0}{\partial y^2}+\dfrac{\partial w}{\partial y}\dfrac{\partial^2 w}{\partial y^2}\right)\\+(A_{12}+A_{66})\left(\dfrac{\partial^2 u_0}{\partial x\partial y}+\dfrac{\partial w}{\partial x}\dfrac{\partial^2 w}{\partial x\partial y}\right)\\+A_{66}\left(\dfrac{\partial^2 v_0}{\partial x^2}+\dfrac{\partial w}{\partial y}\dfrac{\partial^2 w}{\partial x^2}\right)+A_{31}^e\dfrac{\partial \phi}{\partial y}\end{pmatrix}=I_0\frac{\partial^2 v_0}{\partial t^2} \tag{27.2}$$

$$\begin{pmatrix}k_sA_{44}\left(\dfrac{\partial^2 w}{\partial x^2}+\dfrac{\partial^2 w}{\partial y^2}+\dfrac{\partial \psi_x}{\partial x}+\dfrac{\partial \psi_y}{\partial y}\right)\\-k_sE_{15}^e\left(\dfrac{\partial^2 \phi}{\partial x^2}+\dfrac{\partial^2 \phi}{\partial y^2}\right)\\-N^E\left(\dfrac{\partial^2 w}{\partial x^2}+\dfrac{\partial^2 w}{\partial y^2}\right)+Z_1+Z_2\end{pmatrix}=I_0\frac{\partial^2 w}{\partial t^2} \tag{27.3}$$

$$\begin{pmatrix} D_{11}\dfrac{\partial^2\psi_y}{\partial y^2}+D_{12}\dfrac{\partial^2\psi_x}{\partial x\partial y} \\ +D_{66}\left(\dfrac{\partial^2\psi_y}{\partial x^2}+\dfrac{\partial^2\psi_x}{\partial x\partial y}\right) \\ +(E_{31}^e+k_sE_{15}^e)\dfrac{\partial\phi}{\partial y} \\ +k_sA_{44}\left(\dfrac{\partial w}{\partial y}+\psi_y\right) \end{pmatrix}=I_2\frac{\partial^2\psi_y}{\partial t^2} \tag{27.4}$$

$$\begin{pmatrix} E_{15}^e\left(\dfrac{\partial^2 w}{\partial x^2}+\dfrac{\partial^2 w}{\partial y^2}+\dfrac{\partial\psi_x}{\partial x}+\dfrac{\partial\psi_y}{\partial y}\right) \\ +E_{31}^e\left(\dfrac{\partial^2\psi_x}{\partial x^2}+\dfrac{\partial^2\psi_y}{\partial y^2}\right) \\ +X_{11}^e\left(\dfrac{\partial^2\phi}{\partial x^2}+\dfrac{\partial^2\phi}{\partial y^2}\right)-X_{33}^e\phi \end{pmatrix}=0 \tag{27.5}$$

$$\begin{aligned} Z_1=&\begin{bmatrix} A_{11}\left(\dfrac{\partial u_0}{\partial x}+\dfrac{1}{2}\left(\dfrac{\partial w}{\partial x}\right)^2\right) \\ +A_{12}\left(\dfrac{\partial v_0}{\partial y}+\dfrac{1}{2}\left(\dfrac{\partial w}{\partial y}\right)^2\right) \end{bmatrix}\left(\frac{\partial^2 w}{\partial x^2}\right) \\ &+\begin{bmatrix} A_{11}\left(\dfrac{\partial^2 u_0}{\partial x^2}+\dfrac{\partial w}{\partial x}\dfrac{\partial^2 w}{\partial x^2}\right) \\ +A_{12}\left(\dfrac{\partial^2 v_0}{\partial x\partial y}+\dfrac{\partial w}{\partial y}\dfrac{\partial^2 w}{\partial x\partial y}\right) \end{bmatrix}\left(\frac{\partial w}{\partial x}\right) \\ &+\begin{bmatrix} A_{12}\left(\dfrac{\partial u_0}{\partial x}+\dfrac{1}{2}\left(\dfrac{\partial w}{\partial x}\right)^2\right) \\ +A_{11}\left(\dfrac{\partial v_0}{\partial y}+\dfrac{1}{2}\left(\dfrac{\partial w}{\partial y}\right)^2\right) \end{bmatrix}\left(\frac{\partial^2 w}{\partial y^2}\right) \\ &+\begin{bmatrix} A_{12}\left(\dfrac{\partial^2 u_0}{\partial x\partial y}+\dfrac{\partial w}{\partial x}\dfrac{\partial^2 w}{\partial x\partial y}\right) \\ +A_{11}\left(\dfrac{\partial^2 v_0}{\partial y^2}+\dfrac{\partial w}{\partial y}\dfrac{\partial^2 w}{\partial y^2}\right) \end{bmatrix}\left(\frac{\partial w}{\partial y}\right) \end{aligned} \tag{27.6}$$

$$\begin{aligned} Z_2=&2A_{66}\left(\frac{\partial u_0}{\partial y}+\frac{\partial v_0}{\partial x}+\frac{\partial w}{\partial x}\frac{\partial w}{\partial y}\right)\frac{\partial^2 w}{\partial x\partial y} \\ &+A_{66}\left(\frac{\partial^2 u_0}{\partial x\partial y}+\frac{\partial^2 v_0}{\partial x^2}+\frac{\partial w}{\partial y}\frac{\partial^2 w}{\partial x^2}+\frac{\partial w}{\partial x}\frac{\partial^2 w}{\partial x\partial y}\right)\frac{\partial w}{\partial y} \\ &+A_{66}\left(\frac{\partial^2 u_0}{\partial y^2}+\frac{\partial^2 v_0}{\partial x\partial y}+\frac{\partial w}{\partial y}\frac{\partial^2 w}{\partial x\partial y}+\frac{\partial w}{\partial x}\frac{\partial^2 w}{\partial y^2}\right)\frac{\partial w}{\partial x} \end{aligned} \tag{27.7}$$

Here, considering the electric potentials that are zero at the edges of smart piezo-electrically actuated plates, i.e., $\phi = 0$, the expressions of the piezo-electrically actuated sandwich plates with various boundary conditions (B.Cs) could be described as:

a) The smart sandwich plate that is piezoelectrically activated and has all clamped edges:

$$\begin{aligned} &u=v=w=\psi_x=\psi_y=\phi=0 \\ &at\ x=0,a\ and\ y=0,b \end{aligned} \tag{28.1}$$

b) Smart piezoelectrically-activated sandwich plate with completely simply-supported edges:

$$\begin{aligned} &u=v=w=\phi=0 \\ &at\ x=0,a\ and\ y=0,b \\ &M_{xx}=\psi_y=0\ at\ x=0,a \end{aligned} \tag{28.2}$$

$$\psi_x=M_{yy}=0\ at\ y=0,b$$

3. Solution method

3.1 Discretization on the space domain

The GDQM is a proper procedure for detecting the mechanical performance of structures. This expression may be used to express the *m*th derivative of the displacement field:

$$\frac{\partial^m f(x)}{\partial x^m}=\sum_{k=1}^{n} C_{ik}^{(m)} f(x) \tag{29}$$

In addition, the Kronecker tensor product (represented by $\otimes$) may be used to approximately describe the partial derivative of the corresponding function *f (x, y)* on the fields.

$$\frac{\partial^{m+n} f(x,y)}{\partial x^m\partial y^n\left(C_y^{(n)}\otimes C_x^{(m)}\right)(x,y)} \tag{30}$$

In which m and n denote the grid coordinates on the *x* and *y* axis, respectively, utilizing the Chebyshev Gauss Lobatto cosine pattern grid distribution, the GDQ grid points yield the following equation (Wang 2015):

$$\begin{aligned} x_i&=\tfrac{1}{2}\left(1-cos\left(\tfrac{(i-1)}{(m-1)}\pi\right)\right)i=1,2,3,\ldots,m \\ y_i&=\tfrac{1}{2}\left(1-cos\left(\tfrac{(j-1)}{(n-1)}\pi\right)\right)j=1,2,3,\ldots,n \end{aligned} \tag{31}$$

Differentials of the discrete forms are substituted into the governing equations, giving:

$$[\boldsymbol{K}_L+\boldsymbol{K}_{NL}]d+[\boldsymbol{M}]\frac{d^2 d}{dt^2}=0 \tag{32}$$

Additionally, the linear and nonlinear stiffness matrixes can be presented by K_L and K_{NL} in that order. Also, the mass matrix denoted by $M.M, KL$, and KNL are all $6N_xN_y \times 6N_xN_y$ matrixes.

3.2 Derivation of Duffing-type equations

By replacing the $d^* = d.e^{i\omega}$ into Eq. (32), the eigenvalue system is represented as:

$$([\boldsymbol{K}_L+\boldsymbol{K}_{NL}]-\omega^2[\boldsymbol{M}])\{d\}=0 \tag{33}$$

And *d* would be represented as follows:

$$\{d\}=\{u,v,w,\psi_x,\psi_y,\phi\}^T \tag{34}$$

Initially, by ignoring ***(KNL)*** in Eqs. (27). The eigenvalue and eigenvector can be derived from the linear equations, and the eigenvector is scaled up and denoted by w_{max}^* . Then and there, estimate the nonlinear terms of equations (***KNL)*** via the linear eigenvectors, and then new eigenvalue and eigenvector can be derived from the new nonlinear Eq. (35). This process often continues until the discrepancy between two successive eigenvalue calculations is smaller than$(1e^{-4})$.

$$|[\boldsymbol{K}_L+\boldsymbol{K}_{NL}]-\omega^2[\boldsymbol{M}]|=0 \tag{35}$$

Table 1 Material characteristics $BaTiO_3$ and $CoFe_2O_4$

characteristics	$BaTiO_3$	$CoFe_2O_4$
$c_{11} = c_{22}$ (GPa)	166	286
c_{33}	162	269.5
$c_{13} = c_{23}$	78	170.5
c_{12}	77	173
c_{55}	43	45.3
c_{66}	44.5	56.5
e_{31} (Cm^{-2})	-4.4	0
e_{33}	18.6	0
e_{15}	11.6	0
s_{11} $(10^{-9}C^2m^{-2}N^{-1})$	11.2	0.08
s_{33}	12.6	0.093
ρ (kgm^{-3})	5800	5300
Auxetic Core		
$\theta = 55$ $E_{Al} = 70$GPa	$\theta = 55$ $E_{Al} = 70$GPa	$\theta = 55$ $E_{Al} = 70$GPa

Table 2 The natural frequency of a plate with a rectangular shape is compared to that of numerous BC as a function of h/b

B.C	C-C-C-C		S-S-S-S		S-C-S-C	
h/b	[33]	Current study	[33]	Current study	[33]	Current study
0.001	35.98	36.477	19.74	20.387	28.95	29.474
0.1	32.49	33.339	19.06	19.751	26.65	27.411
0.2	26.46	27.649	17.43	18.189	22.32	23.329

Table 3 Compared of (ω_{nl}/ω_l) of a rectangular plate via SSSS B.C. (a/h=1000)

w/h	Chu and Herrmann (1956)	Sundararajan *et al.* (2005)	Liu *et al.* (2016)	Balamurugan *et al.* (1996)	Present study
0.2	1.0260	1.0256	1.0267	1.0254	1.0273
0.4	1.1003	1.0992	1.1013	1.0982	1.1041
0.6	1.2140	1.2126	1.2118	1.2119	1.2187
0.8	1.3574	1.3566	1.3467	1.3558	1.3591
1.0	1.5219	1.5234	1.4987	1.5200	1.5164

4. Discussion and analysis

4.1 Tables

This part of article presents Tables and Figures that illustrate the nonlinear vibrations of the smart NPR cellular sandwich plate under various boundary conditions (C-C-C-C, S-S-S-S, C-C-C-S, C-C-S-S, and C-S-S-S).

The plate includes the smart composite layers and NPR cellular core. Furthermore, the factors of the smart NPR cellular composite plate are generally assumed to be as below:

Also, the material of the NPR cellular core is presumed to be (AL). Moreover, the parameters of the auxetic core and electro-mechanical layers (filler and matrix) are presented in Table 1.

The first natural frequencies of a plate via a rectangular shape are offered in Table 2 based on Liew *et al.* (1998) for different boundary conditions and aspect ratios. The second table exhibits that the present study is in concordance with Liew *et al.* (1998). The nonlinear frequency ratio of the rectangular plate for the SSSS boundary condition (B.C.) and several nonlinear vibration amplitudes ($W_{max}= w/h$) is shown in Table 3 of a separate study. This validation demonstrates that this comparison perfectly matches the references by Sundararajan *et al.* (2005), Chu and Herrmann (1956), and Balamurugan *et al.* (1996).

4.2 Figures

Fig. 2 illustrates that the smart sandwich plate's (ω_{nl}/ω_l) varies according to the nonlinear vibration amplitude W_{max} for various geometrical parameters (b) as displayed in these figures (ω_{nl}/ω_l) rises as W_{max} grows to 1. The (ω_{nl}/ω_l) improves significantly by increasing the geometrical parameter (b) from 1 to 4 in S-S-S-S and C-

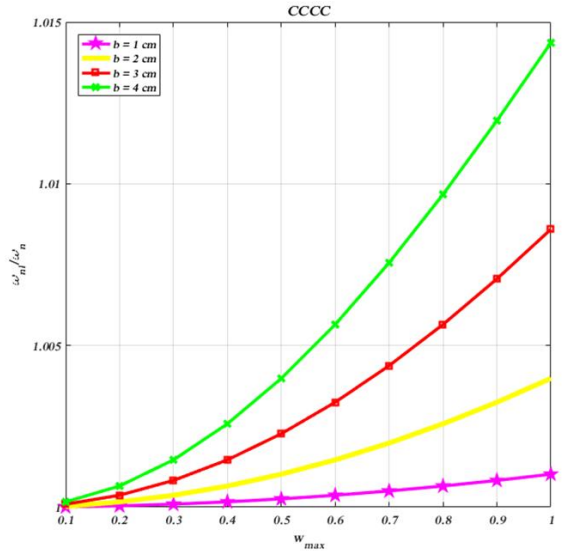

(a) C-C-C-C boundary condition

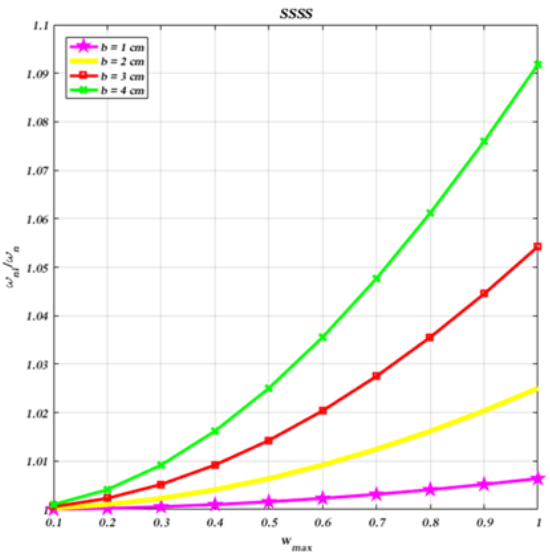

(b) S-S-S-S boundary condition

Fig. 2 Effect of the various geometrical parameters (b) on $(\boldsymbol{\omega_{nl}/\omega_l})$of a piezo-electrically actuated plate

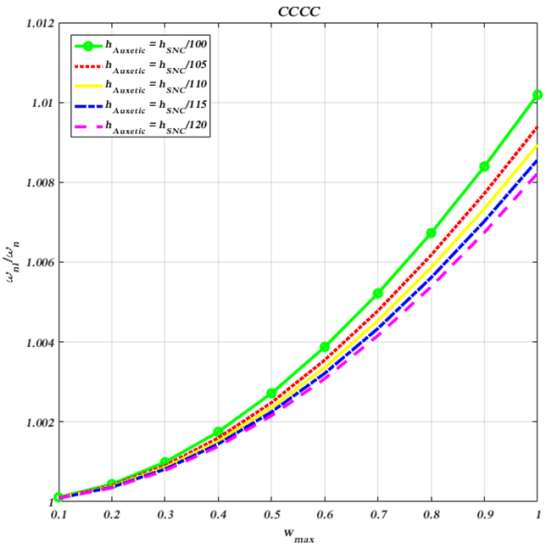

(a) C-C-C-C boundary condition

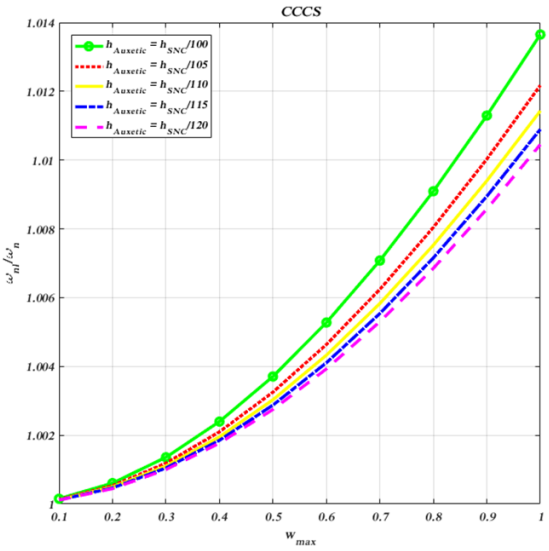

(b) C-C-C-S boundary condition

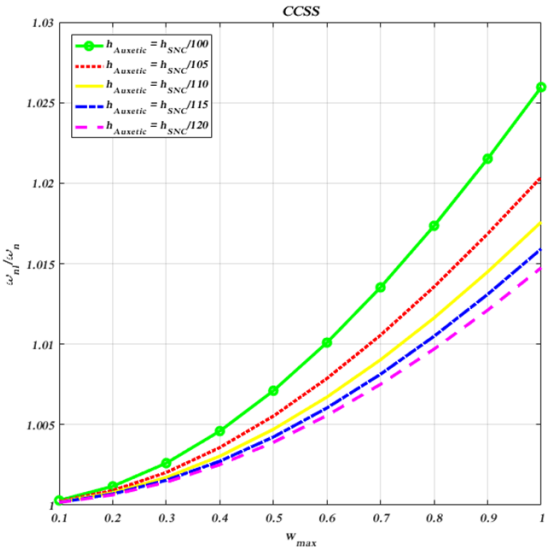

(c) C-C-S-S boundary condition

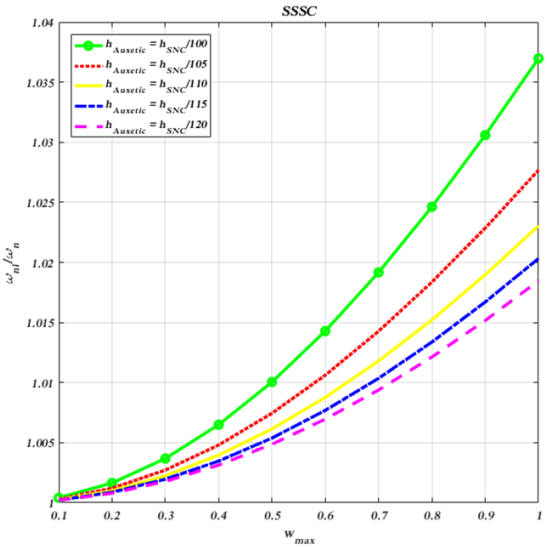

(d) S-S-S-C boundary condition

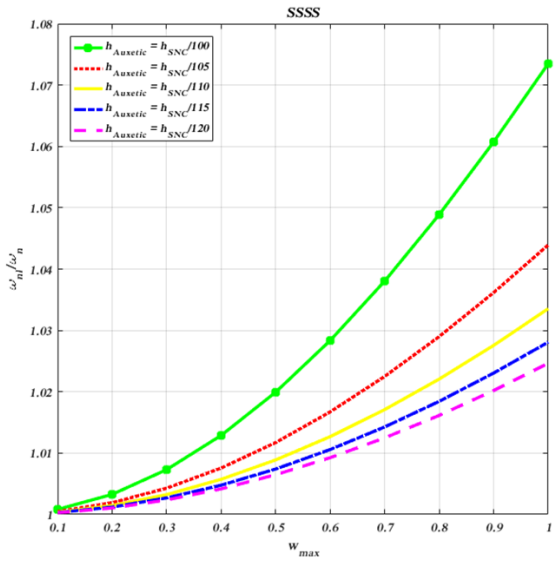

(e) S-S-S-S boundary condition

Fig. 3 Effect of numerous depths of NPR cellular core ($\boldsymbol{h_{Auxetic}}$) on $(\boldsymbol{\omega_{nl}/\omega_l})$ of a piezo-elect plate

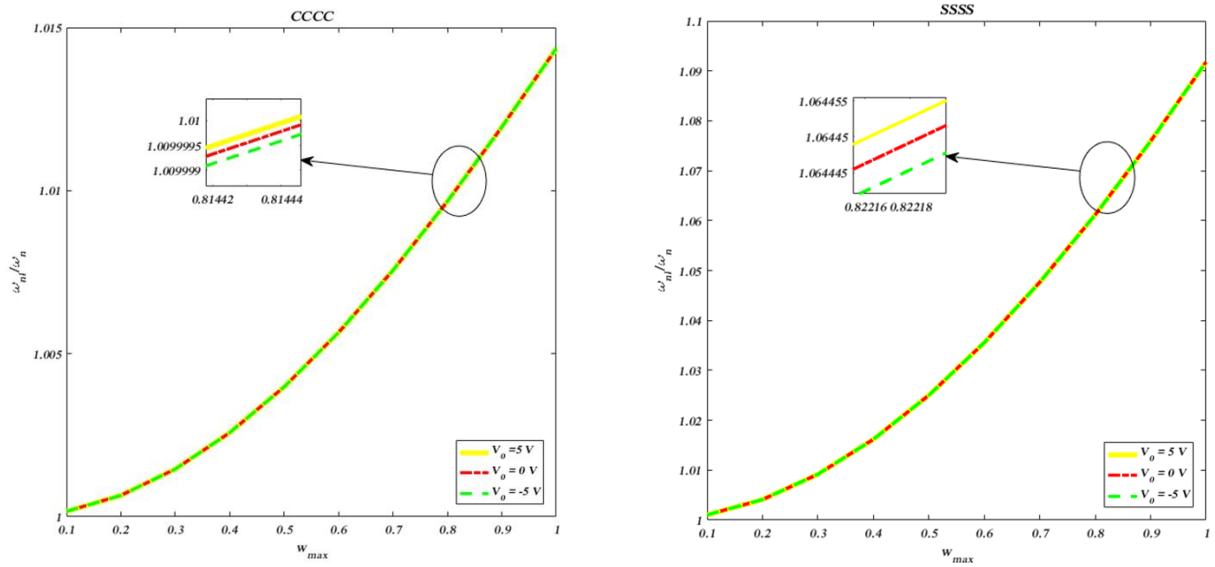

(a) C-C-C-C boundary condition (b) S-S-S-S boundary condition

Fig. 4 Influence of outside voltage $(\boldsymbol{V_0})$ on $(\boldsymbol{\omega_{nl}/\omega_l})$ of a piezo-electrically actuated plate

C-C-C BCs. Additionally, the variance of (ω_{nl}/ω_l)in S-S-S-S boundary conditions is greater than in C-C-C-C BC. Nonlinear hardening is shown via a smart NPR cellular sandwich plate. This result shows that when the dimensional amplitude increases, the hardening nonlinearity of the smart NPR cellular sandwich plate grows. It is shown that the smart NPR cellular sandwich plate's hardening nonlinearity rises as its geometrical parameters (b) expand.

Fig. 3 depicts a smart sandwich plate's (ω_{nl}/ω_l) changes as a function of nonlinear vibration amplitude W_{max} for various NPR cellular core thicknesses. As shown in these figures, the (ω_{nl}/ω_l) rises as the nonlinear vibration's amplitude W_{max} grows to 1. By decreasing the thickness of the NPR cellular core from $h_{SC}/120$ to $h_{SC}/100$, the (ω_{nl}/ω_l) is significantly increased. The influence of BC on the difference of (ω_{nl}/ω_l) is excessively evident to be S-S-S-S > S-S-S-C > S-S-C-C > S-C-C-C > C-C-C-C. Nonlinear hardening is shown using a smart NPR cellular sandwich plate. This result reveals that the hardening nonlinearity of the smart NPR cellular composite plate improves via an increase in dimensionless amplitude. Smart NPR cellular sandwich plates are found to have a greater hardening nonlinearity as their NPR cellular core thicknesses grow.

Fig. 4 illustrates the (ω_{nl}/ω_l) variations of a smart composite plate as a function of nonlinear vibration magnitude W_{max} for varying outside voltage (V_0). As shown in these figures, as W_{max} grows from 0.1 to 1, the (ω_{nl}/ω_l) is raised. By increasing the external voltage (V_0) in S-S-S-S and C-C-C-C boundary conditions, the (ω_{nl}/ω_l)

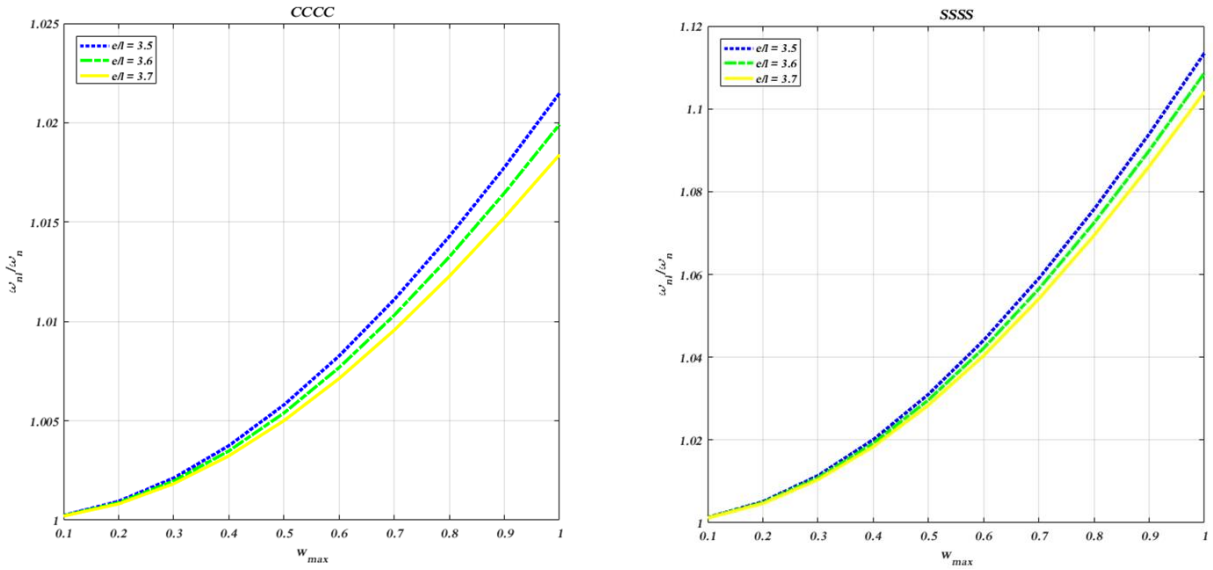

(a) C-C-C-C boundary condition (b) S-S-S-S boundary condition

Fig. 5 Effect of the various values of $(\boldsymbol{e/l})$ on the $(\boldsymbol{\omega_{nl}/\omega_l})$ of a piezo-electrically actuated plate

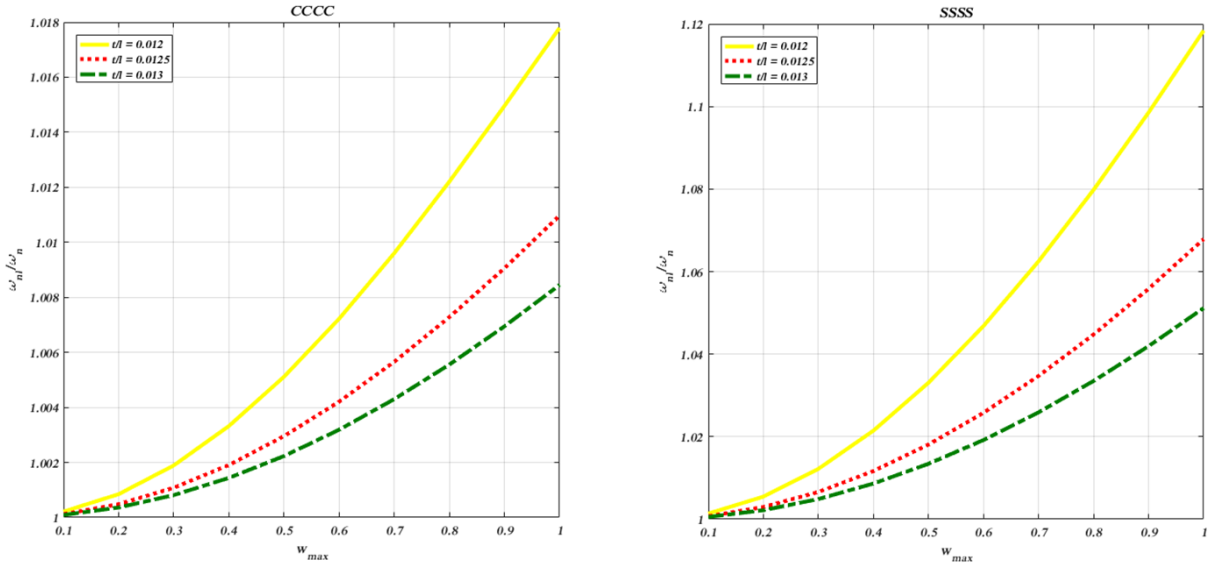

(a) C-C-C-C boundary condition (b) S-S-S-S boundary condition

Fig. 6 Impact of various parameters in geometry $(\boldsymbol{t/l})$ on $(\boldsymbol{\omega_{nl}/\omega_l})$ of a piezo-electrically actuated plate

grows noticeably. It is readily apparent that the deviation of the (ω_{nl}/ω_l) in S-S-S-S B.C is greater than in C-C-C-C B.C.

Fig. 5 illustrates the (ω_{nl}/ω_l)variations of a smart sandwich plate due to nonlinear amplitudes of vibration W_{max} for different geometrical variables (e/l) as exposed in these figures, (ω_{nl}/ω_l) rises as the nonlinear vibration magnitude W_{max} rises from 0.1 to 1. By decreasing the distinct geometrical parameters (e/l) in S-S-S-S and C-C-C-C B.Cs, the value of (ω_{nl}/ω_l)increases noticeably. The variance of (ω_{nl}/ω_l) in S-S-S-S B.C. exceeds the C-C-C-C boundary condition. A smart NPR cellular sandwich plate was constructed to demonstrate nonlinear hardening. This finding demonstrates that increasing the dimensionality-free amplitude of the smart NPR cellular sandwich plate enhances its hardening nonlinearity. It is shown that when the geometrical parameters (e/l) of the smart NPR cellular sandwich plate decrease, so does the hardening nonlinearity of the material.

Fig. 6 depicts a smart sandwich plate's (ω_{nl}/ω_l) change due to nonlinear vibration magnitude W_{max} for various geometrical variables (t/l) as presented in these figures, (ω_{nl}/ω_l) rises as the nonlinear vibration magnitude W_{max} grows from 0.1 to 1. By decreasing the geometrical coefficient (t/l) from 0.013 to 0.012 in S-S-S-S and C-C-C-C B.Cs., the value of (ω_{nl}/ω_l) increases significantly. The variation of (ω_{nl}/ω_l) in SSSS boundary conditions may be greater than in C-C-C-C B.C. Nonlinear hardening is shown via a smart NPR cellular sandwich plate. This result reveals that an increase in dimensionless

amplitude increases the hardening nonlinearity of the smart NPR cellular sandwich plate. The hardening nonlinearity of the smart NPR cellular sandwich plate is demonstrated to increase when the geometrical parameter (t/l) is lowered.

5. Conclusions

The present study using the Mindlin plate theory to characterize the electro-mechanical behavior of nonlinear vibration for smart sandwich rectangular plates. These outcomes provide a comprehensive understanding of how geometrical and material parameters affect the nonlinear dynamic behavior of smart sandwich plates. Such insights can be instrumental in the optimal design of adaptive structures utilized in mechanical, and civil engineering applications, where vibration control and lightweight performance are critical. The material of the smart sandwich plate with piezoelectrically actuated composite layers consists of a NPR cellular core and two composite layers. Using micromechanics models, the homogenization of smart piezoelectrically composite layers is planned. Furthermore, the nonlinear governing equations and corresponding B.Cs. (GDQM) is used to tackle the smart sandwich plate's problems. At this juncture, a summary of the greatest highlights can be described as follows:

• (ω_{nl}/ω_l) decreases with increasing thicknesses of the NPR cellular core, plate length, and external voltage increase.

• The value of (ω_{nl}/ω_l) rises when the nonlinear vibration amplitude W_{max} rises.

• The hardening effect grows with the thickness of the NPR cellular core in various BCs.

• The ratio of nonlinear to linear frequency(ω_{nl}/ω_l) increases with the growth of vibration amplitude W_{max}, indicating a hardening the nonlinear behavior of the system.

• For higher values of geometric ratios such as $^{e}/_{l}$ and $^{t}/_{l}$,the magnitude of this frequency ratio decreases, despite the overall increasing trend of the curve. This means that the intensity of the hardening effect weakens as these geometric parameters grow.

• The influence of boundary conditions (BCs) is clearly visible in the frequency response curves, in certain configurations, their impact is comparatively insignificant and thus may not be a primary design concern compared to the dominant effects of geometric or electric parameters.

Future studies can extend this work by including temperature-dependent behavior, imperfections, or different piezoelectric control schemes. Additionally, experimental validation of the proposed models would further confirm their applicability in real-world engineering systems

Acknowledgments

The authors would like to thank the referees for their valuable comments. Additionally, we would like to express our gratitude to the University of Tehran, and Imam Khomeini International University for their support and resources provided throughout this research.

The authors declare that there are no financial or personal conflicts of interest regarding this manuscript.

References

Balamurugan, V., Ganapathi, M. and Varadan, T.K. (1996), "Nonlinear dynamic instability of laminated composite plates using finite element method", *Comput. Struct.*, **60**(1), 125-130. https://doi.org/10.1016/0045-7949(96)00044-9.

Chen, J., Yang, J. and Kitipornchai, S. (2017), "Nonlinear aeroelastic flutter and dynamic response of composite laminated cylindrical shell in supersonic air flow", *Compos. Struct.*, **168**, 474-484. https://doi.org/10.1016/j.compstruct.2017.02.019.

Cheng, Y.F. (2011), "A comparison of large deflections of circular plates with different boundary conditions", *Struct. Eng. Mech.*, **91**(4), 1301-1328. https://doi.org/10.12989/sem.2011.91.4.1301.

Cheng, Y.F. and Xu, B.M. (2013a), "A comparison of large deflections of FGM Plates", *Steel Compos. Struct.*, **91**(4), 1301-1328. https://doi.org/10.12989/scs.2013.91.4.1301.

Cheng, Y.F. and Xu, B.M. (2013b), "A comparison of large deflections of composite plates", *J. Wing Eng.*, **91**(4), 1301-1328. https://doi.org/10.12989/xxx.2013.91.4.1301.

Cheng, Y.F., Xu, B.M. and Carter, G.D. (2012), "A comparison of large deflections of rectangular plates with different boundary conditions", *Comput. Concr.*, **91**(4), 1301-1328. https://doi.org/10.12989/cac.2012.91.4.1301.

Ebrahimi, F. and Barati, M.R. (2016), "A nonlocal higher-order refined magneto-electro-viscoelastic beam model for dynamic analysis of smart nanostructures", *Int. J. Eng. Sci.*, **107**, 183-196. https://doi.org/10.1016/j.ijengsci.2016.07.005.

Ebrahimi, F. and Dabbagh, A. (2019), *Wave Propagation Analysis of Smart Nanostructures*, CRC Press, Boca Raton, FL, U.S.A.

Ebrahimi, F. and Rastgoo, A. (2009), "Nonlinear vibration of smart circular functionally graded plates coupled with piezo-electric layers", *Int. J. Mech. Mater. Des.*, **5**(2), 157-165. https://doi.org/10.1007/s10999-009-9067-3.

Ebrahimi, F. and Zia, M. (2015), "Large amplitude nonlinear vibration analysis of functionally graded Timoshenko beams with porosities", *Acta Astronaut.*, 1-12. https://doi.org/10.1016/j.actaastro.2015.05.021.

Evans, K.E. (1991), "Auxetic materials", *Nature*, **353**, 10065. https://doi.org/10.1038/353451a0.

Ghorbanpour Arani, A., Jamali, M., Ghorbanpour-Arani, A.H., Kolahchi, R. and Mosayyebi, M. (2017), "Electro-magneto wave propagation analysis of viscoelastic sandwich nanoplates considering surface effects", *Proc. Inst. Mech. Eng. Part C J. Mech. Eng. Sci.*, **231**(2), 387-403. https://doi.org/10.1177/0954406216639531.

Hosseini, M., Mahinzare, M. and Ghadiri, M. (2018), "Magnetic field effect on vibration of a rotary smart size-dependent two-dimensional porous functionally graded nanoplate", *Eur. Phys. J. Plus*, **132**(3), 115. https://doi.org/10.1140/epjp/i2017-11544-2.

Hua, L. and Lam, K.Y. (2001), "Orthotropic influence on frequency characteristics of a rotating composite laminated conical shell by the generalized differential quadrature method", **38**(1), 3995-4015. https://doi.org/10.1007/978-1-4864-2075-8_9

Huang, Y., Yang, L.E. and Luo, Q.Z. (2013), "Free vibration of axially functionally graded timoshenko beams with non-uniform cross-section", *Compos. Part B Eng.*, **45**(1), 1493-1498. https://doi.org/10.1016/j.compositesb.2013.04.007.

Ilkhani, M.R. and Hosseini-Hashemi, S.H. (2016), "Size dependent vibro-buckling of rotating beam based on modified couple stress theory", *Compos. Struct.*, **143**, 75-83. https://doi.org/10.1016/j.compstruct.2016.03.074.

Jafari, A.A., Khalili, S.M.R. and Tavakolian, M. (2014), "Nonlinear vibration of functionally graded cylindrical shells embedded with a piezoelectric layer", *Thin-Walled Struct.*, **79**, 8-15. https://doi.org/10.1016/j.tws.2014.01.013.

Jiang, L. and Hu, H. (2017), "Low-velocity impact response of multilayer orthogonal structural composite with auxetic effect", *Compos. Struct.*, **169**, 62-68. https://doi.org/10.1016/j.compstruct.2017.03.043.

Liew, K.M., Xiang, Y., Kitipornchai, S. and Wang, C. (1998), *Vibration of Mindlin Plates: Programming the p-version Ritz Method*, Elsevier.

Liu, C., Ke, L.L., Yang, J., Kitipornchai, S. and Wang, Y.S. (2016), "Nonlinear vibration of piezoelectric nanoplates using nonlocal mindlin plate theory", *Mech. Adv. Mater. Struct.*, **6494**. https://doi.org/10.1080/15376494.2016.1174834.

Mahinzare, M., Jannat, M., Abbas, S. and Ghadiri, M. (2019), "A nonlocal strain gradient theory for dynamic modeling of a rotary thermo piezo electrically actuated nano FG circular plate", *Mech. Syst. Signal Proc.*, **115**, 323-337. https://doi.org/10.1016/j.ymssp.2018.06.014.

Mahinzare, M., Rastgoo, A. and Ebrahimi, F. (2022), "On nonlinear vibration of piezo-electrically multi-scale hybrid nanocomposite sandwich plate including an auxetic core based on HSDT", *Int. J. Struct. Stab. Dyn.*, **23**(4), 2250025. https://doi.org/10.1142/S0219455422500255.

Mahinzare, M., Rastgoo, A. and Ebrahimi, F. (2024), "Nonlinear vibration of FG graphene origami auxetic sandwich plate including smart hybrid nanocomposite sheets", *J. Eng. Mech.*, **150**(4), 04024007. https://doi.org/10.1061/JENMDT.EMENG-7398

Malekzadeh, P. (2008), "Differential quadrature large amplitude free vibration analysis of laminated skew plates based on FSDT", *Compos. Struct.*, **83**(2), 189-200. https://doi.org/10.1016/j.compstruct.2007.04.004.

Mohammadpour, M. and Taheri-Behrooz, F. (2024), "Compressive and flexural responses of auxetic sandwich panels with modified sre-entrant honeycomb cores", *J. Sandw. Struct. Mater.*, **26**(7), 1165-1181. https://doi.org/10.1177/10996362231161631.

Nguyen, D.D. and Pham, C.H. (2018), "Nonlinear dynamic response and vibration of sandwich composite plates with negative poisson's ratio in auxetic honeycombs", *J. Sandw. Struct. Mater.*, **20**(6), 692-717. https://doi.org/10.1177/1099636217713700.

Quan, T.Q., Anh, V.M., Mahesh, V. and Duc, N.D. (2020), "Vibration and nonlinear dynamic response of imperfect sandwich piezoelectric auxetic plate", *Mech. Adv. Mater. Struct.*, 1-11. https://doi.org/10.1080/15376494.2020.1741046.

Rachid, E.K., Khalid, E.B. and Rhali, B. (2014), "A semi-analytical study of geometrically nonlinear free axisymmetric vibrations of thin circular functionally graded plates using iterative and explicit analytical solution", *Appl. Mech. Mater.*, **704**, 131-136. https://doi.org/10.4028/www.scientific.net/AMM.704.131.

Ranjbar, M., Boldrin, L., Scarpa, F., Neild, S. and Patsias, S. (2016), "Vibroacoustic optimization of anti-tetrachiral and auxetic hexagonal sandwich panels with gradient geometry", *Smart Mater. Struct.*, **25**(5). https://doi.org/10.1088/0964-1726/25/5/055004.

Reddy, J.N. (2006), *Theory and Analysis of Elastic Plates and Shells*, CRC Press, Boca Raton, FL, USA.

Shariyat, M., Khaghani, M. and Lavasani, S.M.H. (2010), "Nonlinear thermoelasticity, vibration, and stress wave propagation analyses of thick FGM cylinders with temperature-dependent material properties", *Eur. J. Mech. A Solids*, **29**(3), 378-391. https://doi.org/10.1016/j.euromechsol.2009.10.008.

Shen, H.S. and Xiang, Y. (2014), "Nonlinear vibration of nanotube-reinforced composite cylindrical panels resting on elastic foundations in thermal environments", *Compos. Struct.*, **111**, 291-300. https://doi.org/10.1016/j.compstruct.2014.01.056.

Sundararajan, N., Prakash, T. and Ganapathi, M. (2005), "Nonlinear free flexural vibrations of functionally graded rectangular and skew plates under thermal environments", *Finite Elem. Anal. Des.*, **42**(2), 152-168. https://doi.org/10.1016/j.finel.2005.06.001

Wang, X. (2015), *Differential Quadrature and Differential Quadrature-Based Element Methods: Theory and Applications*, Butterworth-Heinemann, Oxford, U.K.

Wang, K., Chang, Y.H., Chen, Y.W., Zhang, C. and Wang, B. (2015), "Designable dual-material auxetic metamaterials using three-dimensional printing", *Mater. Des.*, **67**, 159-164. https://doi.org/10.1016/j.matdes.2014.11.039.

Yang, W., Li, Z.M., Shi, W., Xie, B.H. and Yang, M.B. (2004), "On auxetic materials", *J. Mater. Sci.*, **39**(10), 3269-3279. https://doi.org/10.1023/B:JMSC.0000030911.95974.9a.

Yazdani Sarvestani, H., Akbarzadeh, A.H., Niknam, H. and Hermenean, K. (2018), "3D printed architected polymeric sandwich panels: Energy absorption and structural performance", *Compos. Struct.*, **200**, 886-909. https://doi.org/10.1016/j.compstruct.2018.05.022.

CC